

DeepPortraitDrawing: Generating Human Body Images from Freehand Sketches

XIAN WU, Tsinghua University
 CHEN WANG, Tsinghua University
 HONGBO FU, City University of Hong Kong
 ARIEL SHAMIR, The Interdisciplinary Center
 SONG-HAI ZHANG, Tsinghua University
 SHI-MIN HU*, Tsinghua University

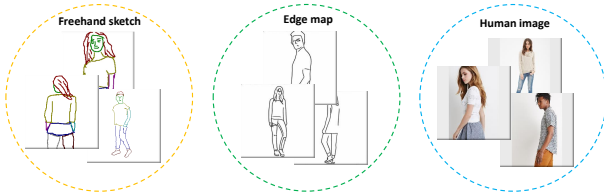


Fig. 1. There are huge gaps between freehand sketches with human images and the extracted edge maps. The freehand sketches, especially by those with few drawing skills, might not describe the local geometry or global structure of a human body accurately.

Researchers have explored various ways to generate realistic images from freehand sketches, e.g., for objects and human faces. However, how to generate realistic human body images from sketches is still a challenging problem. It is, first because of the sensitivity to human shapes, second because of the complexity of human images caused by body shape and pose changes, and third because of the domain gap between realistic images and freehand sketches. In this work, we present *DeepPortraitDrawing*, a deep generative framework for converting roughly drawn sketches to realistic human body images. To encode complicated body shapes under various poses, we take a local-to-global approach. Locally, we employ semantic part auto-encoders to construct part-level shape spaces, which are useful for refining the geometry of an input pre-segmented hand-drawn sketch. Globally, we employ a cascaded spatial transformer network to refine the structure of body parts by adjusting their spatial locations and relative proportions. Finally, we use a global synthesis network for the sketch-to-image translation task, and a face refinement network to enhance facial details. Extensive experiments have shown that given roughly sketched human portraits, our method produces more realistic images than the state-of-the-art sketch-to-image synthesis techniques.

ACM Reference format:

Xian Wu, Chen Wang, Hongbo Fu, Ariel Shamir, Song-Hai Zhang, and Shi-Min Hu. 2022. *DeepPortraitDrawing: Generating Human Body Images from Freehand Sketches*. 1, 1, Article 1 (May 2022), 10 pages. <https://doi.org/10.1145/nnnnnnn.nnnnnnn>

1 INTRODUCTION

Creating realistic human images benefits various applications, such as fashion design, movie special effects, and educational training. Generating human images from freehand sketches can be more effective since even non-professional users are familiar with such a

pen-and-paper paradigm. Sketches can not only represent the global structure of a human body but also depict the local appearance details of the body as well as garments.

Deep generative models, such as generative adversarial networks (GANs) [Goodfellow et al. 2014] and variational auto-encoders (VAEs) [Kingma and Welling 2013], have recently made a breakthrough for image generation tasks. Based on these generative models, many methods [Chen and Hays 2018; Isola et al. 2017; Lu et al. 2018; Sangkloy et al. 2017] have been proposed to generate desired images from input sketches by solving a general image-to-image translation problem. Some other methods have focused on generating specific types of images, including human faces [Chen et al. 2020; Li et al. 2020] and foreground objects [Ghosh et al. 2019]. Such methods can better handle freehand sketches by incorporating the relevant domain knowledge.

Compared to many other types of images, human body images have more complicated intrinsic structures and larger shape and pose variations, making the sketch-based synthesis task difficult for the following reasons. First, existing human portrait image datasets [Liu et al. 2016] only cover a small subset of all possible human images under various changing conditions of pose, shape, view-point, and garment. Since the existing sketch-to-image translation techniques often use pairs of images and their corresponding edge maps for training, they may fail to generate desired results when a test sketch is under very different conditions. Second, hand-drawn sketches, especially those created by users with little drawing skills, can hardly describe accurate body geometry and structure, and look very different from edge maps extracted from the training images (Figure 1).

In this work, we present *DeepPortraitDrawing*, a novel deep generative approach for generating realistic human images from coarse, rough freehand sketches (Figure 2). Instead of trying to increase the generalization ability of sketch-to-image algorithms, our key idea is to project an input test sketch to part-level shape spaces constructed based on image-based training data. This can assist to bridge the gap between the training and test data, and also the gap between freehand sketches and realistic images. This idea makes sense for our task since roughly drawn sketches do not provide hard constraints for geometric interpretation. By properly recombining part-level information in different training images we are able to cover a significant portion of all possible human images.

To this end, we take a local-to-global approach to encode complicated body shapes under various poses. For each semantic body

*Corresponding Author

part, we employ an auto-encoder to define a part-level latent shape space by training on part-level edge maps extracted from images. Our system takes as input a semantically segmented sketch, whose individual body parts are projected onto the constructed part-level shape spaces. This results in a geometrically refined sketch map and a corresponding parsing map (i.e., labeled regions). Next, we employ a cascaded spatial transformer network to structurally refine the sketch and parsing maps by adjusting the locations and relative proportions of individual body parts. Finally, we use a global synthesis network to produce a realistic human image from the transformed maps, and use a face refinement network to improve the local details of facial landmarks.

Extensive experiments demonstrate the effectiveness and practicality of our method. We are able to satisfy novice users' need for creating visually pleasing human images from hand-drawn sketches. In our self-collected dataset of freehand sketches, our method produces visually more pleasing results with more realistic local details, compared to the previous sketch-based image generation techniques (Figure 7). The main contributions of our paper can be summarized as follows:

- We are the first to consider the problem of synthesizing realistic human images from roughly drawn sketches;
- We present a local-to-global deep generative solution to geometrically and structurally refine an input sketched human before image synthesis.
- We collect a hand-drawn sketch dataset of human images (containing 308 segmented sketches), which can facilitate future research.

2 RELATED WORK

2.1 Sketch-to-image generation

Generating desired images from hand-drawn sketches is a difficult task, since sketches often exhibit different levels of abstraction. To address this domain gap, traditional methods take a *retrieval-composition* approach, essentially considering sketches as soft constraints. For example, a pioneering work by Chen et al. [2009] first retrieves images from the Internet using input sketches with text descriptions, and fuses the retrieved foreground and background images into desired pictures. A similar idea is used in PhotoSketcher [Eitz et al. 2011]. PoseShop [Chen et al. 2013] constructs image scenes with human figures but requires users to provide 2D poses for retrieval. Since such retrieval-based approaches directly reuse portions of existing images for re-composition, their performance is highly dependent on the scale of image datasets, as well as the composition quality.

By using deep learning models, (e.g., conditional GANs [Mirza and Osindero 2014]), recent sketch-based image synthesis works adopt a *reconstruction*-based approach. Some works [Isola et al. 2017; Wang et al. 2018a; Zhu et al. 2017a] aim at general-purpose image-to-image translation and can handle sketches as one of the possible input types. Other works focus on using sketches as the condition for GANs. For example, Scribbler [Sangkloy et al. 2017] can control textures in generated images by grayscale sketches and colorful strokes. Contextual-GAN [Lu et al. 2018] updates latent vectors for input sketches through back propagation and produces

images by a pre-trained model. SketchyGAN [Chen and Hays 2018] and iSketchNFill [Ghosh et al. 2019] are able to generate multi-class images for diverse sketches by introducing gated conditions. Gao et al. [2020] propose an approach to produce scene images from sketches, by generating each foreground object instance and the background individually. Recently, Ho et al. [2020] propose a coarse-to-fine generation framework and incorporate human poses to synthesize human body images. While impressive results were presented in the above works, these techniques do not generalize well to rough or low-quality sketches, which have very different characteristics compared to image edge-maps used for training the generative models. Additionally, since sketches are largely used as hard constraints in these techniques, the synthesized images would inherit geometric distortions if they exist in the input sketches (Figure 7).

Our approach has been inspired by the recent work DeepFaceDrawing [Chen et al. 2020], which takes a *projection-reconstruction* approach for synthesizing realistic human face images from sketches. The key idea of DeepFaceDrawing is to refine the input sketches before synthesizing the final image. This refinement is achieved by projecting the input sketches to component-level spaces spanned by edge maps of realistic faces. DeepFaceDrawing achieves impressive results even for rough or incomplete sketches but is limited to the synthesis of frontal faces. We extend their approach to synthesizing human body images under various poses and viewpoints. Our extension explicitly uses the semantic information in the whole pipeline, and contributes a spatial transformation module, essentially leading to a *projection-transformation-reconstruction* pipeline.

2.2 Label-to-image generation

There are many semantic synthesis approaches generating images from segmentation label maps. For example, Pix2pix [Isola et al. 2017] is a general image-to-image translation framework based on a U-Net [Ronneberger et al. 2015] generator and a conditional discriminator. Chen and Koltun [2017] present a cascaded refinement network and use multi-layer perceptual losses to achieve photographic images from segmentation maps. Pix2pixHD [Wang et al. 2018a] employs multi-scale generators and discriminators, and incorporates a feature matching loss to build a high-resolution image-to-image translation framework. GauGAN [Park et al. 2019] introduces the SPADE layer to control image styles directly by semantic segmentation. Zhu et al. [2020] present a semantically multi-modal synthesis model to generate images with diverse styles for each semantic label. LGGAN [Tang et al. 2020b] combines local class-specific sub-generators and a global image-level generator for semantic scene generation. DAGAN [Tang et al. 2020a] present two novel attention modules to capture spatial-wise and channel-wise attention individually. Different from the above *reconstruction*-based approaches, Qi et al. [2018] introduce a *retrieval-reconstruction* image synthesis method. They retrieve image segments from a dataset using segmentation maps as query and employ a global refinement network to produce globally consistent results. Although segmentation labels can be used to generate plausible images, they are less expressive than sketches in describing local details and geometric textures of user-desired images. (e.g., collars and sleeves in Figure 7)

2.3 Human body image generation

Human-body image synthesis is challenging, because of human sensitivity to human shapes. There is a need to make the global body structure reasonable and to produce realistic local textures. Most researchers have focused on the human pose transfer task [Ma et al. 2017, 2018], which synthesizes the same person from a source image in target poses. To achieve this, some methods utilize component masks [Balakrishnan et al. 2018; Siarohin et al. 2018], human parsing [Dong et al. 2018; Han et al. 2019], or correspondence flows [Li et al. 2019b; Liu et al. 2019a; Ren et al. 2020] to transform local source features into target areas, thus preserving the appearance of the same person in target poses. Other methods [Lassner et al. 2017; Neverova et al. 2018] employ dense pose [Alp Güler et al. 2018] or statistical human models like SMPL [Loper et al. 2015] to provide the human body structure as a prior. Several methods [Liu et al. 2019b; Neverova et al. 2018; Sarkar et al. 2020] construct a surface texture map from a source human body image, and then render the texture map on a target human image. Recently, HumanGAN [Sarkar et al. 2021] proposes novel part-based encoding and warping modules for generating diverse human images with high quality. These pose transfer techniques focus on preserving texture details from source images, while our method focuses on generating body textures and garments according to hand-drawn sketches.

Besides pose, other approaches synthesize human images by modifying other properties. For example, FashionGAN [Zhu et al. 2017b] encodes the shape, appearance, and text, allowing to edit garment textures of human images through text descriptions. Many researchers have attempted to address the virtual try-on problem [Han et al. 2018; Wang et al. 2018b], i.e., dressing a source person with given clothes through proper geometric transformations. Ak et al. [2019] and Men et al. [2020] use attribute vectors to represent appearance information and then control the clothes and textures of human images via such attribute vectors. Dong et al. [2020] leverage a parsing map as guidance and introduce an attention normalization layer to edit human images by sketches and colors. These methods are able to change certain properties for a source human image, but they cannot generate a brand-new human image from scratch.

3 METHOD

We propose a *projection-transformation-reconstruction* approach for generating realistic human body images from freehand sketches. As illustrated in Figure 2, it is achieved through three modules operated in sequence: a geometry refinement module, a structure refinement module, and an image generation module. The geometry refinement module takes a semantically segmented sketch as input and refines the geometry of its individual body parts by retrieving and interpolating the exemplar body parts in the latent spaces of the learned part-level auto-encoders. This module results in a refined sketch map and a corresponding parsing map. The structure refinement module spatially transforms the sketch and parsing maps to better connect and shape individual parts, and refine the relative proportions of body parts. Finally, the image generation module translates the transformed maps into a realistic human body image.

3.1 Geometry refinement module

This module aims to refine an input freehand sketch by using human portrait images to train several part-level networks. This has two advantages. First, locally pushing the input sketch towards the training edge maps, and second reducing the geometric errors in the input sketch. This assists the image generation module in generating more realistic images.

Due to the complexity of human images, it is very unlikely to find in our training dataset an image that is globally similar to an input sketch (Figure 7). On the other hand, it is much easier to retrieve similar body parts and learn a component-level shape space for each body part. We thus follow the idea in DeepFaceDrawing [Chen et al. 2020] to perform manifold projection at the component level.

DeepFaceDrawing has focused on the synthesis of frontal faces and relies on a shadow interface to guide users to sketch face components that are well aligned with the training examples. This alignment is critical for synthesizing realistic faces with DeepFaceDrawing. In contrast, we aim to handle portrait images under various poses and viewpoints. Hence, we cannot use a single layout template for body components. Instead, we propose to use the semantic segmentation information through the entire pipeline, since semantic labels provide a natural way to establish corresponding body parts in different images.

Let S denote a test sketch or a training edge map. We assume that S has been semantically segmented into $C = 8$ parts, including hair, face, top-clothes, bottom-clothes, left and right arms, left and right legs. We denote the part sketches as $\{S^c\}_{c=1,\dots,C}$. Each body part S^c is cropped by a corresponding bounding box (S^c will be a white image if part- c is absent from S). We use an auto-encoder architecture to extract a feature vector for each body part to facilitate the subsequent manifold projection task, as illustrated in Figure 2.

In the testing stage, given a semantically segmented sketch denoted as $\{S^c\}_{c=1,\dots,C}$, we project its body parts to the underlying part-level manifolds for geometric refinement. We adopt the Locally Linear Embedding (LLE) algorithm [Roweis and Saul 2000] to perform manifold projection without explicitly constructing each part-level manifold. Specifically, each part sketch S^c is first encoded into a latent vector v^c by a corresponding encoder E^c . Based on the local linear assumption, we use a retrieve-and-interpolate approach. In more detail, we first retrieve K nearest neighbors $\{v_k^c\}_{k=1,\dots,K}$ for v^c in the latent space $\{v_i^c\}$ for part c using the Euclidean distance. $\{v_i^c\}$ collected from a set of training images can be considered as the samples that build the underlying part-level manifold for part c . We then interpolate the retrieved neighbors to approximate v^c by minimizing the mean squared error as follows:

$$\min \|v^c - \sum_{k=1}^K w_k^c \cdot v_k^c\|_2^2, \quad s.t. \sum_{k=1}^K w_k^c = 1, \quad (1)$$

where $K = 10$ in our experiments and w_k^c is the unknown weight of the k -th vector candidate. For each body part, $\{w_k^c\}$ can be found independently by solving a constrained least-squares problem. After the weights $\{w_k^c\}$ are found, we can calculate the projected vector

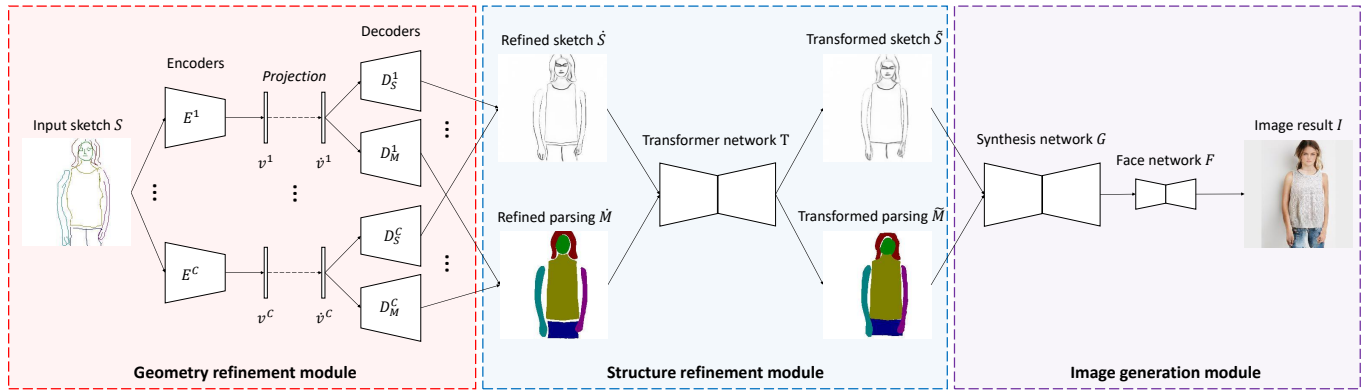


Fig. 2. Pipeline of the proposed *projection-transformation-reconstruction* approach to generate human body images from freehand sketches. Firstly, individual body parts of an input sketch are projected onto the underlying part-level manifolds and decoded into a geometrically refined sketch map and a parsing map, based on an auto-encoder architecture. Secondly, the individual parts of the refined sketch map and the parsing map are transformed via a cascaded spatial transformer network, to refine the global structure of the human body. Thirdly, the transformed maps are fed into the global synthesis network to generate a new human image and then the face refinement network to enhance the facial details.

\hat{v}^c by linear interpolation:

$$\hat{v}^c = \sum_{k=1}^K w_k^c \cdot v_k^c. \quad (2)$$

Next, the sketch decoder D_S^c and the mask decoder D_M^c for part c process the projected vector \hat{v}^c , resulting in a refined part sketch \hat{S}^c and a part mask \hat{M}^c , respectively. Finally, all projected part sketches $\{\hat{S}^c\}$ and masks $\{\hat{M}^c\}$ are combined together to recover the global body shape, resulting in a geometry-refined sketch map \hat{S} and a human parsing map \hat{M} .

In the training stage, we first train the encoder E^c and the sketch decoder D_S^c to avoid the distraction from the mask branch. Since E^c and D_S^c need to reconstruct the input S^c with consistent shapes and fine details, we employ the L_2 distance as the reconstruction loss to train them. Then, we fix the weights of the parameters in E^c and train the mask decoder D_M^c . We use the cross-entropy loss for this training since it is a binary segmentation task.

3.2 Structure refinement module

The geometry refinement module focuses only on the refinement of the geometry of individual body parts in a sketch. However, relative positions and proportions between body parts in a hand-drawn sketch might not be accurate. We thus employ the structure refinement module to refine the relative positions and proportions of body parts to get a globally more consistent body image.

To refine the body structure, we use the pose keypoints (see Figure 3), which provide a simple and effective way to represent a human body structure. According to the physiological characteristics of human beings, the positions of pose keypoints should obey two rules. First, a joint of a body part should connect to the same joint of its neighboring body part. Second, the relative length of different body parts should be globally consistent. Therefore, we aim to transform the keypoints of different body parts and make them conform to these rules.

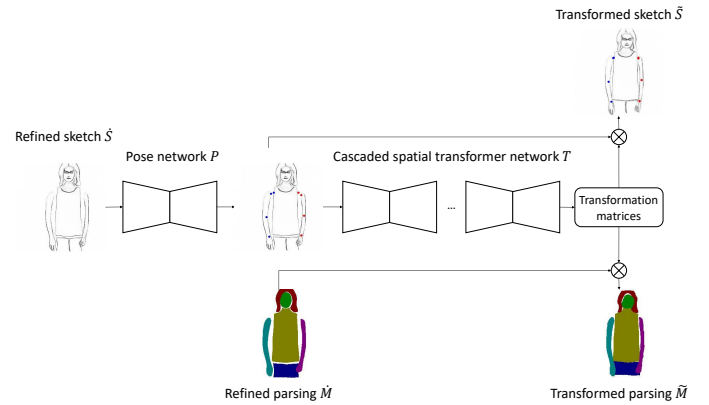


Fig. 3. Illustration of the structure refinement module. The keypoints of individual body parts (e.g., the arms and shoulders) are better connected and their relative length is globally more consistent after this step.

As illustrated in Figure 3, we first utilize a pose estimation network P to predict heatmaps H^c for the position of each keypoint from each refined part sketch map \hat{S}^c . Note that we need to predict the same joint repeatedly for neighboring body parts. Then, we leverage all the part heatmaps $\{H^c\}$ as guidance to recover the global structure of the sketched human body. The different body parts should preserve proper relative lengths, and connect with each other based on the inherent relationships among them. To achieve this, we apply affine transformations to the body parts predicted by a spatial transformer network [Jaderberg et al. 2015] T , so that the part heatmaps $\{H^c\}$ are transformed to reasonable locations $\{\hat{H}^c\}$ learned from real human poses. We apply the same predicted affine transformations to the refined part sketch maps $\{\hat{S}^c\}$ and the part mask maps $\{\hat{M}^c\}$, resulting in $\{\tilde{S}^c\}$ and $\{\tilde{M}^c\}$, respectively.

Since neighboring body parts may influence each other, it is very difficult to recover the entire human structure in one step

transformation. Therefore, we use a cascaded refinement strategy, employing a multi-step spatial transformer network to update the results iteratively. To leverage the global information, we combine all the part sketch maps as \hat{S} and all the part heatmaps as H , and then feed \hat{S} and H to the spatial transformer network. The transformed sketch map \tilde{S} and heatmaps \tilde{H} in the j -th step are the input to the transformer network in the $(j + 1)$ -th step. In our experiments, we used a three-step refinement, as illustrated in Figure 4.

To train the pose estimation network P and the cascaded spatial transformer network T , we need to simulate the inconsistencies of the global structure we may find at the test time. We apply random affine transformations to all part edge maps $\{S^c\}$ and part heatmaps $\{H^c\}$ in the training set, except for a selected reference part. We select the top-clothes part (i.e., the upper body) as the reference part and keep it unchanged in our experiments. The pose network P needs to predict all part heatmaps $\{\hat{H}^c\}$ from each randomly transformed edge map \hat{S} . We adopt the stacked hourglass architecture [Newell et al. 2016] for P and use the mean squared error to train it.

The goal of the cascaded spatial transformer network T is to refine the size and location of each body part. Therefore, the predicted pose heatmaps $\{\hat{H}^c\}$ should be transformed so that they are as close to the ground-truth $\{H^c\}$ as possible. Similarly, we require the randomly transformed part edge maps $\{\hat{S}^c\}$ to be close to the ground-truth part edge maps $\{S^c\}$. We have found that extremely large transformations may lead to training instability. We thus append a regularization term to penalize transformation matrices that are too large. The spatial transformer network T_{j+1} in the $(j + 1)$ -th step is fed with the transformed edge map \hat{S}_j and the combined heatmaps \hat{H}_j in the j -th step. Its initial input is \hat{S}_0 and \hat{H}_0 . The loss function of T can be formulated as:

$$\begin{aligned} \mathcal{L}(T) = & \sum_{j=0}^2 \sum_{c=1}^C \lambda_H \|\mathcal{F}(T_{j+1}^c(\hat{S}_j, \hat{H}_j), \hat{H}_j^c) - H^c\|_2^2 \\ & + \lambda_S \|\mathcal{F}(T_{j+1}^c(\hat{S}_j, \hat{H}_j), \hat{S}_j^c) - S^c\|_2^2 \\ & + \lambda_L \|T_{j+1}^c(\hat{S}_j, \hat{H}_j) - \mathbb{I}\|_2^2, \end{aligned} \quad (3)$$

where \mathcal{F} represents an affine transformation operation and \mathbb{I} denotes the identity matrix. $T_{j+1}^c(\hat{S}_j, \hat{H}_j)$ denotes the predicted transformation matrix for the c -th body part in the $(j + 1)$ -th step. We set $\lambda_H = 100$ and $\lambda_S = \lambda_L = 1$ in our experiment to balance the three terms.

3.3 Image generation module

Finally, we need to generate a desired human image I from the transformed sketch map \tilde{S} and the transformed parsing map \tilde{M} after the structure refinement module, as illustrated in Figure 5. We adopt GauGAN [Park et al. 2019] as our basic architecture for the global synthesis network G , since it has achieved impressive results for the label-to-image translation task. The SPADE layer in GauGAN [Park et al. 2019] takes the parsing map \tilde{M} as input by default. To prevent losing the information in the sketch map \tilde{S} , we concatenate it to the parsing map \tilde{M} and feed them together into the SPADE layer. This way, the parsing map \tilde{M} controls the image style in each semantic region, while the sketch map \tilde{S} provides the geometric features for local details.

The global synthesis network G is able to generate an acceptable result \tilde{I} globally. However, the human visual system is more sensitive to the quality of synthesized faces. Since hand-drawn human body sketches might not describe facial landmarks clearly, G may fail to produce rich details for the face area. Inspired by Chan et al. [2019], we utilize a face refinement network F to enhance the facial details in the human image \tilde{I} . We crop a square patch from \tilde{I} according to the face label in \tilde{M} . The square patch and the face mask are then fed into the face refinement network F to produce a residual image for the face area. The final result I is the sum of \tilde{I} and the residual image. To train F to achieve a realistic human face, we adopt both an adversarial loss and a perceptual loss, similar to Chan et al. [2019].

To train the global synthesis network G , we could simply take the edge maps $\{S_i\}$ and the parsing maps $\{M_i\}$ in the training set as input. However, we have found that the synthesis network G trained this way cannot address freehand sketches well. Although the geometry refinement module can refine the geometric shape of an input sketch S , the resulting sketch \hat{S} still differs from edge maps found in the training set. The main reason is that edge maps extracted from natural human images contain many texture details, and these can violate the local linear assumption [Roweis and Saul 2000] used in the step of manifold projection. Instead, to simulate the input at the test time, we take the projected version of each edge map in the training set as the input to train G . We retrieve K nearest neighbors in the underlying manifold for each edge map S_i . Then, the edge maps $\{\hat{S}_i\}$ and the parsing maps $\{\hat{M}_i\}$ decoded by the projected vectors are fed into G . Similar to GauGAN [Park et al. 2019], we adopt the adversarial loss, the perceptual loss, and the feature matching loss [Wang et al. 2018a] together to train G .

4 EXPERIMENTS

To get the paired data for training, we construct a large-scale sketch dataset of human images from DeepFashion [Liu et al. 2016], as described in Sec 4.1. Sec 4.2 introduces the architecture of our proposed networks and the implementation details of model training. We conduct comparison experiments with several sketch-to-image techniques in Sec 4.3 to show the superiority of our method for generating human images from hand-drawn sketches. The ablation study in Sec 4.4 evaluates the contribution of individual components in our method. Sec 4.5 shows that our method is able to produce multi-style human images from the same input sketches.

4.1 Data preparation

Training the global synthesis network G needs a dataset of paired images and sketches. Similar to previous methods [Chen et al. 2020; Isola et al. 2017; Sangkloy et al. 2017], we extract edge maps from human images of 256×256 resolution in DeepFashion [Liu et al. 2016] to build our synthetic sketch dataset. At first, we filter the DeepFashion dataset to remove images of the lower body. Then we apply the edge detection method proposed by Im2Pencil [Li et al. 2019a] to get an edge map for each human image (Figure 6 from (a) to (b)). By employing the sketch simplification method proposed by Simo-Serra et al. [2018], we clean noise curves in the extracted edge maps (Figure 6 (c)) so they resemble hand-drawn sketches more. This results in a new large-scale sketch dataset of human images

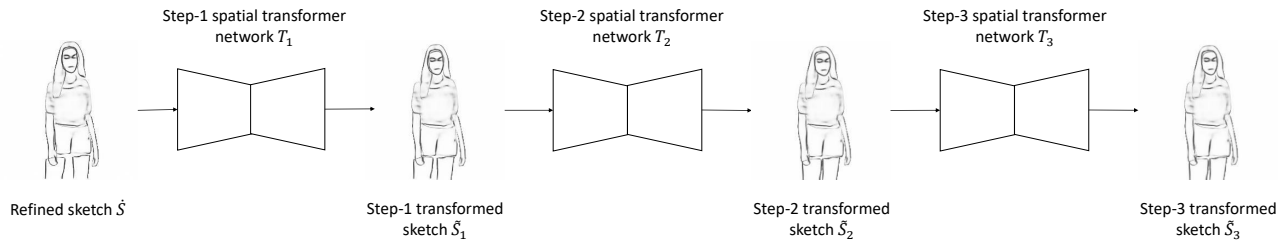


Fig. 4. In our experiments, a geometrically refined sketch map \hat{S} is transformed iteratively for three steps to get a structurally refined sketch map.

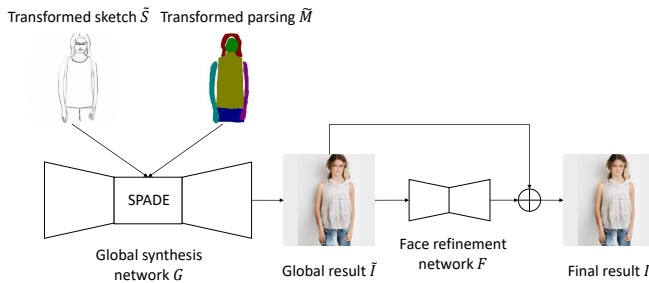


Fig. 5. Illustration of the image generation module. The transformed sketch and parsing maps are fed into the SPADE layer of the global synthesis network to produce a human image result. Then the face refinement network enhances the facial details for the final result.

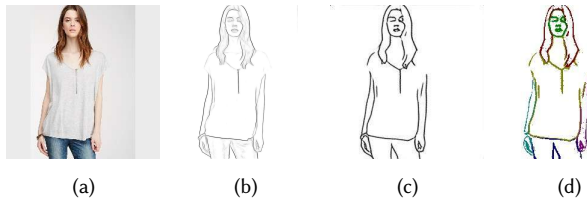


Fig. 6. The process of building our training and validation sets of sketches. (a): Input human image. (b): Edge extraction of (a) by Im2Pencil [Li et al. 2019a]. (c): Sketch simplification of (b) by the method of Simo-Serra et al. [2018]. (d): Part segmentation of (c) by PGN [Gong et al. 2018].

with paired data. This dataset contains 37,844 pairs in total. We randomly select 2,000 pairs as the validation set and the remaining 35,844 pairs as the training set.

Our models also require human parsing maps and pose heatmaps for training. We utilize PGN [Gong et al. 2018] to predict a parsing map for each human image in our dataset. To simplify the problem, we merge several labels in the parsing maps, resulting in $C = 8$ types of body parts altogether. The merged parsing maps are regarded as the ground-truth. These maps also allow us to segment the paired edge maps to obtain semantically segmented edge maps (Figure 6 (d)). To prepare the data for training the transformer network, we first employ OpenPose [Cao et al. 2019] to predict the 2D pose keypoints from the human images, and then generate pose heatmaps from the keypoints based on the Gaussian distribution to better capture spatial features.

To evaluate the usefulness of our method in practice, we have collected freehand sketches from 12 users (6 males, 6 females). Four of them have good drawing skills, while the others are less proficient. The users were asked to imitate a given human image or just draw an imagined human. They were instructed to draw a segmented sketch part by part, taking around one minute to complete one sketch on average. We have collected 308 hand-drawn sketches of human images in total to construct our test set. We plan to release our dataset of paired human images and synthetic edge maps as well as hand-drawn sketches publicly for future research.

4.2 Implementation details

In the geometry refinement module. We share the left and right arms/legs with the same auto-encoders by leveraging the human body symmetry, so there are in total 6 part auto-encoders. Each part encoder E^c contains five downsampling convolutional layers, with each downsampling layer followed by a residual block. A fully-connected layer is appended in the end to encode the features into the latent vector v^c of 512 dimensions. Similarly, the part decoders D_S^c and D_M^c each contain five upsampling convolutional layers and five residual blocks in total. The final convolutional layers in D_S^c and D_M^c reconstruct the part sketch S^c and the part mask M^c , respectively. To train the structure refinement module, we preprocess the training set by applying random affine transformations, which are composed of translation, rotation, resizing, and shearing transformations. The spatial transformer network T_j in each step consists of five downsampling convolutional layers, five residual blocks, and the last two fully-connected layers to predict the affine transformation matrices for all body parts.

We use the Adam [Kingma and Ba 2014] solver to train all the networks. We set the learning rate to 0.0002 initially and linearly decay it to 0 after half iterations. For each part auto-encoder, we first train the encoder E^c and the sketch decoder D_S^c for 100 epochs and then train the mask decoder D_M^c for 50 epochs. We train the pose estimation network P and the cascaded spatial transformer network T both for 50 epochs. We set the batch size to 16 for the above networks. We train the global synthesis network G for 100 epochs of batch size 8 and the face refinement network F for 10 epochs of batch size 10. We conduct the experiments by using an Intel(R) Core(TM) i7-4770 CPU @ 3.40GHz with 4 cores and NVidia GTX 1080 Ti GPUs. Please refer to the supplementary materials for more training and architecture details.

4.3 Comparison with state-of-the-art methods

To demonstrate the effectiveness of our method for synthesizing realistic human images from freehand sketches, we compare our method with four state-of-the-art sketch-based image synthesis methods, including pix2pix [Isola et al. 2017], pix2pixHD [Wang et al. 2018a], GauGAN [Park et al. 2019] and DAGAN [Tang et al. 2020a]. For a fair comparison, we train all the four models on our training set for the same epochs as our method. Please note that we employ the first-stage generator of pix2pixHD [Wang et al. 2018a], since the image resolution of our dataset is limited to 256×256 . We also compare our method with a sketch-based image retrieval approach. To achieve this, we train an auto-encoder for an entire edge map and collect all latent vectors in the training set. Given an input sketch, we encode it into a vector and retrieve the nearest neighbor from the training set. We regard the human image corresponding to the nearest vector as the retrieval result. To eliminate the influence of facial areas, we remove the face enhancement module in our method for comparison.

Figure 7 shows several representative results of our method and the other five approaches on our test sketches. Compared to the four state-of-the-art sketch-to-image synthesis techniques, our method performs much better with visually more pleasing results. Even when the face enhancement module is removed, our method still produces more realistic texture details and more reasonable body structures, owing to the geometry and structure refinement guided by the semantic parsing maps. Compared to the sketch-based image retrieval approach, our method can produce brand-new human images which respect user inputs more faithfully. Please refer to the supplementary materials for more comparison results.

To further evaluate the results, we have applied FID [Heusel et al. 2017] as a quantitative metric, which measures perceptual distances between generated images and real images. Table 1 shows that our method outperforms the other three sketch-to-image synthesis methods [Isola et al. 2017; Park et al. 2019; Wang et al. 2018a], indicating more realistic results by our method. However, as claimed by [Chen et al. 2020], this perceptual metric might not measure the quality of results correctly, since it does not take the geometry and structure of the human body into consideration. Therefore, we also conducted a user study to compare our method with the three sketch-to-image synthesis techniques [Isola et al. 2017; Park et al. 2019; Wang et al. 2018a]. We randomly selected 30 sketches from the test set and showed each sketch along with the four results by the compared methods in a random order to users, who were asked to pick the most realistic results. There were 17 participants in total, resulting in 510 votes. Our method received significantly more votes than the other methods, as shown in Table 1. The participants were also asked to give a score of faithfulness for each result by GauGAN [Park et al. 2019] (we select it as the representative one of the sketch-to-image synthesis methods), the sketch-based image retrieval method, and our method. The scores ranged from 1 to 10, the higher the better. Table 1 shows that the results of our method conform with input sketches better than the image retrieval method and are comparable to GauGAN [Park et al. 2019]. For a fair comparison, we also removed the face enhancement module in our method to produce the results used in the user study.

Table 1. Quantitative evaluation of our method, three sketch-based image synthesis methods [Isola et al. 2017; Park et al. 2019; Wang et al. 2018a], and an image retrieval method. We have used FID [Heusel et al. 2017] as a quantitative metric and conducted a user study to evaluate the realism and faithfulness of the results. The arrow after each metric identifies the improvement direction.

| | FID (↓) | Realism (↑) | Faithfulness (↑) |
|-----------------|--------------|---------------|------------------|
| Pix2pix | 71.12 | 7.65% | / |
| Pix2pixHD | 70.87 | 21.37% | / |
| GauGAN | 51.92 | 24.71% | 6.21 |
| Image retrieval | / | / | 5.18 |
| Our method | 50.36 | 46.27% | 6.15 |

4.4 Ablation study

We have conducted an ablation study to demonstrate the contributions of the different components of our method. Each time, we remove the parsing map guidance, the projection of latent vectors, the spatial transformation, and the face enhancement, respectively, while keeping the other components unchanged. As shown in Figure 8, without the guidance of the human parsing map, our method cannot produce locally consistent results in the same semantic regions (e.g., legs in the second and third rows). Without the projection component, our method cannot refine the geometry of local details, resulting in obvious artifacts. Without the spatial transformation component, our method will produce results with incorrect connection relationships of joints (e.g., shoulders in the second and third rows) or unreasonable body proportions (e.g., the first and fourth rows). Without the face enhancement, our method may not generate realistic facial details.

4.5 Multi-modal synthesis

Similar to previous image-to-image translation methods [Park et al. 2019; Wang et al. 2018a], our method can be easily extended to generate multi-modal human images from the same input sketches. To achieve this, we append an image encoder ahead of the global synthesis network G and train both of them together with an extra KL-divergence loss [Kingma and Welling 2013]. The feature vector encoded by the image encoder can control the texture style of a generated image. Therefore, given the feature vectors encoded by reference human images, our method can produce human images with texture styles similar to the reference images (Figure 9a). Besides, given random feature vectors, our method can also produce diverse human images with different texture styles (Figure 9b).

5 CONCLUSION AND FUTURE WORK

We have proposed a *projection-transformation-reconstruction* approach for generating realistic human images from hand-drawn sketches. Our method consists of three modules, including a geometry refinement module, a structure refinement module, and an image generation module. The geometry refinement module plays an important role in converting roughly drawn sketches into semantic sketch maps, which are locally similar to the edge maps of real human images. This successfully bridges the gap between realistic



Fig. 7. Comparison results with a sketch-based image retrieval method and four state-of-the-art sketch-based image synthesis methods [Isola et al. 2017; Park et al. 2019; Tang et al. 2020a; Wang et al. 2018a]. Our method can produce visually more pleasing results even if the face enhancement module is removed.

images and freehand sketches. The structure refinement module locally adjusts spatial connections between body parts and their relative proportions to get a globally more consistent structure. The image generation module produces visually pleasing human images with fine facial details. Comparison experiments have shown that our approach outperforms three state-of-the-art sketch-to-image synthesis methods, which cannot address freehand sketches well.

Still, the geometry and structure refinement modules are restricted to the data distribution in the training set. Therefore, our method cannot produce human images which are very different from the images in DeepFashion [Liu et al. 2016]. For example, as

shown in Figure 10 (Left), our method generates an unsatisfying result for a hand-drawn sketch of a child. The structure refinement module is also limited to recover the human body structure of an adult only since there are only adult models in DeepFashion [Liu et al. 2016]. As we do not divide the latent vectors of different genders for retrieval, our method is sometimes confused with the gender, as shown in Figure 10 (Right). We will collect more types of human images to improve the generalization ability of our method in the future work. It will also be interesting to introduce colorful strokes to control the texture styles more exactly.



Fig. 8. Comparison results in the ablation study. We remove the parsing map guidance, the projection of latent vectors, the spatial transformation, and the face enhancement in our method, respectively.

REFERENCES

Kenan E Ak, Joo Hwee Lim, Jo Yew Tham, and Ashraf A Kassim. 2019. Attribute manipulation generative adversarial networks for fashion images. In *IEEE International Conference on Computer Vision*. 10541–10550.

Rıza Alp Güler, Natalia Neverova, and Iasonas Kokkinos. 2018. Densepose: Dense human pose estimation in the wild. In *IEEE Conference on Computer Vision and Pattern Recognition*. 7297–7306.

Guha Balakrishnan, Amy Zhao, Adrian V Dalca, Fredo Durand, and John Guttag. 2018. Synthesizing images of humans in unseen poses. In *IEEE Conference on Computer Vision and Pattern Recognition*. 8340–8348.

Z. Cao, G. Hidalgo Martinez, T. Simon, S. Wei, and Y. A. Sheikh. 2019. OpenPose: Real-time Multi-Person 2D Pose Estimation using Part Affinity Fields. *IEEE Transactions on Pattern Analysis and Machine Intelligence* (2019).

Caroline Chan, Shiry Ginosar, Tinghui Zhou, and Alexei A Efros. 2019. Everybody Dance Now. In *IEEE International Conference on Computer Vision*.

Qifeng Chen and Vladlen Koltun. 2017. Photographic image synthesis with cascaded refinement networks. In *IEEE International Conference on Computer Vision*, Vol. 1.

Shu-Yu Chen, Wanchao Su, Lin Gao, Shihong Xia, and Hongbo Fu. 2020. DeepFace-Drawing: deep generation of face images from sketches. *ACM Transactions on Graphics (TOG)* 39, 4 (2020), 72–1.

Tao Chen, Ming-Ming Cheng, Ping Tan, Ariel Shamir, and Shi-Min Hu. 2009. Sketch2photo: Internet image montage. *ACM transactions on graphics (TOG)* 28, 5 (2009), 1–10.

Tao Chen, Ping Tan, Li-Qian Ma, Ming-Ming Cheng, Ariel Shamir, and Shi-Min Hu. 2013. Poseshop: Human image database construction and personalized content synthesis. *IEEE Transactions on Visualization and Computer Graphics* 19, 5 (2013), 824–837.

Wengling Chen and James Hays. 2018. Sketchygan: Towards diverse and realistic sketch to image synthesis. In *IEEE Conference on Computer Vision and Pattern Recognition*. 9416–9425.

Haoye Dong, Xiaodan Liang, Ke Gong, Hanjiang Lai, Jia Zhu, and Jian Yin. 2018. Soft-gated warping-gan for pose-guided person image synthesis. In *Advances in Neural Information Processing Systems*. 474–484.

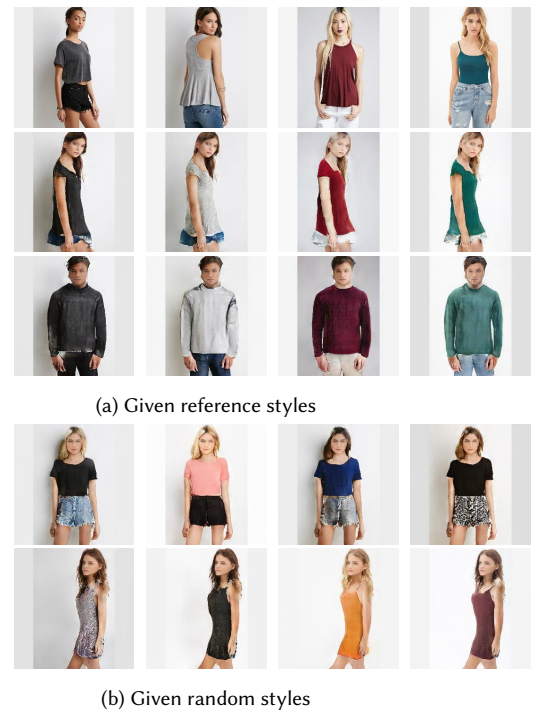


Fig. 9. For a given input sketch, our method can generate multiple results with texture styles similar to the reference images (a) or random styles (b).

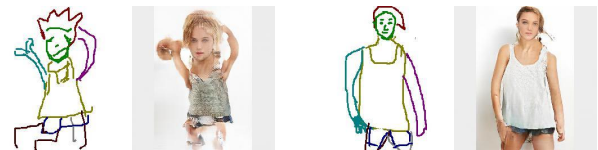


Fig. 10. Less successful cases of our method. Left: our method trained on adult images cannot handle a sketched child well. Right: our method trained on images with mixed genders might fail to respect the gender of an input sketch.

Haoye Dong, Xiaodan Liang, Yixuan Zhang, Xujie Zhang, Xiaohui Shen, Zhenyu Xie, Bowen Wu, and Jian Yin. 2020. Fashion editing with adversarial parsing learning. In *IEEE/CVF Conference on Computer Vision and Pattern Recognition*. 8120–8128.

Mathias Eitz, Ronald Richter, Kristian Hildebrand, Tamy Boubekeur, and Marc Alexa. 2011. Photosketcher: interactive sketch-based image synthesis. *IEEE Computer Graphics and Applications* 31, 6 (2011), 56–66.

Chengying Gao, Qi Liu, Qi Xu, Limin Wang, Jianzhuang Liu, and Changqing Zou. 2020. SketchyCOCO: image generation from freehand scene sketches. In *IEEE/CVF Conference on Computer Vision and Pattern Recognition*. 5174–5183.

Arnab Ghosh, Richard Zhang, Puneet K Dokania, Oliver Wang, Alexei A Efros, Philip HS Torr, and Eli Shechtman. 2019. Interactive sketch & fill: Multiclass sketch-to-image generation. In *IEEE international conference on computer vision*. 1171–1180.

Ke Gong, Xiaodan Liang, Yicheng Li, Yimin Chen, Ming Yang, and Liang Lin. 2018. Instance-level human parsing via part grouping network. In *European Conference on Computer Vision*. 770–785.

Ian Goodfellow, Jean Pouget-Abadie, Mehdi Mirza, Bing Xu, David Warde-Farley, Sherjil Ozair, Aaron Courville, and Yoshua Bengio. 2014. Generative adversarial nets. In *Advances in neural information processing systems*. 2672–2680.

Xintong Han, Xiaojun Hu, Weilin Huang, and Matthew R Scott. 2019. Clothflow: A flow-based model for clothed person generation. In *IEEE International Conference on Computer Vision*. 10471–10480.

- Xintong Han, Zuxuan Wu, Zhe Wu, Ruichi Yu, and Larry S Davis. 2018. Viton: An image-based virtual try-on network. In *IEEE conference on computer vision and pattern recognition*. 7543–7552.
- Maxin Heusel, Hubert Ramsauer, Thomas Unterthiner, Bernhard Nessler, and Sepp Hochreiter. 2017. Gans trained by a two time-scale update rule converge to a local nash equilibrium. In *Advances in neural information processing systems*. 6626–6637.
- Trang-Thi Ho, John Jethro Virtusio, Yung-Yao Chen, Chih-Ming Hsu, and Kai-Lung Hua. 2020. Sketch-guided Deep Portrait Generation. *ACM Transactions on Multimedia Computing, Communications, and Applications (TOMM)* 16, 3 (2020), 1–18.
- Phillip Isola, Jun-Yan Zhu, Tinghui Zhou, and Alexei A Efros. 2017. Image-To-Image Translation With Conditional Adversarial Networks. In *IEEE Conference on Computer Vision and Pattern Recognition*. 1125–1134.
- Max Jaderberg, Karen Simonyan, Andrew Zisserman, et al. 2015. Spatial transformer networks. In *Advances in neural information processing systems*. 2017–2025.
- Diederik P Kingma and Jimmy Ba. 2014. Adam: A method for stochastic optimization. *arXiv preprint arXiv:1412.6980* (2014).
- Diederik P Kingma and Max Welling. 2013. Auto-Encoding Variational Bayes. *arXiv preprint arXiv:1312.6114* (2013).
- Christoph Lassner, Gerard Pons-Moll, and Peter V Gehler. 2017. A generative model of people in clothing. In *IEEE International Conference on Computer Vision*. 853–862.
- Yuhang Li, Xuejin Chen, Binxin Yang, Zihan Chen, Zhihua Cheng, and Zheng-Jun Zha. 2020. DeepFacePencil: Creating Face Images from Freehand Sketches. In *ACM International Conference on Multimedia*. 991–999.
- Yijun Li, Chen Fang, Aaron Hertzmann, Eli Shechtman, and Ming-Hsuan Yang. 2019a. Im2pencil: Controllable pencil illustration from photographs. In *IEEE Conference on Computer Vision and Pattern Recognition*. 1525–1534.
- Yining Li, Chen Huang, and Chen Change Loy. 2019b. Dense intrinsic appearance flow for human pose transfer. In *IEEE Conference on Computer Vision and Pattern Recognition*. 3693–3702.
- Lingjie Liu, Weipeng Xu, Michael Zollhoefer, Hyeonwoo Kim, Florian Bernard, Marc Habermann, Wenzheng Wang, and Christian Theobalt. 2019b. Neural rendering and reenactment of human actor videos. *ACM Transactions on Graphics (TOG)* 38, 5 (2019), 1–14.
- Wen Liu, Zhixin Piao, Jie Min, Wenhan Luo, Lin Ma, and Shenghua Gao. 2019a. Liquid Warping GAN: A Unified Framework for Human Motion Imitation, Appearance Transfer and Novel View Synthesis. In *IEEE International Conference on Computer Vision*.
- Ziwei Liu, Ping Luo, Shi Qiu, Xiaogang Wang, and Xiaoou Tang. 2016. Deepfashion: Powering robust clothes recognition and retrieval with rich annotations. In *IEEE Conference on Computer Vision and Pattern Recognition*. 1096–1104.
- Matthew Loper, Naureen Mahmood, Javier Romero, Gerard Pons-Moll, and Michael J Black. 2015. SMPL: A skinned multi-person linear model. *ACM transactions on graphics (TOG)* 34, 6 (2015), 248.
- Yongyi Lu, Shangzhe Wu, Yu-Wing Tai, and Chi-Keung Tang. 2018. Image generation from sketch constraint using contextual gan. In *European Conference on Computer Vision*. 205–220.
- Liqian Ma, Xu Jia, Qianru Sun, Bernt Schiele, Tinne Tuytelaars, and Luc Van Gool. 2017. Pose guided person image generation. In *Advances in Neural Information Processing Systems*. 405–415.
- Liqian Ma, Qianru Sun, Stamatios Georgoulis, Luc Van Gool, Bernt Schiele, and Mario Fritz. 2018. Disentangled person image generation. In *IEEE Conference on Computer Vision and Pattern Recognition*. 99–108.
- Yifang Men, Yiming Mao, Yuning Jiang, Wei-Ying Ma, and Zhouhui Lian. 2020. Controllable person image synthesis with attribute-decomposed gan. In *IEEE/CVF Conference on Computer Vision and Pattern Recognition*. 5084–5093.
- Mehdi Mirza and Simon Osindero. 2014. Conditional generative adversarial nets. *arXiv preprint arXiv:1411.1784* (2014).
- Natalia Neverova, Riza Alp Guler, and Iasonas Kokkinos. 2018. Dense pose transfer. In *European Conference on Computer Vision*. 123–138.
- Alejandro Newell, Kaiyu Yang, and Jia Deng. 2016. Stacked hourglass networks for human pose estimation. In *European Conference on Computer Vision*. 483–499.
- Taesung Park, Ming-Yu Liu, Ting-Chun Wang, and Jun-Yan Zhu. 2019. Semantic image synthesis with spatially-adaptive normalization. In *IEEE Conference on Computer Vision and Pattern Recognition*. 2337–2346.
- Xiaojuan Qi, Qifeng Chen, Jiaya Jia, and Vladlen Koltun. 2018. Semi-parametric image synthesis. In *IEEE Conference on Computer Vision and Pattern Recognition*. 8808–8816.
- Yurui Ren, Xiaoming Yu, Junming Chen, Thomas H Li, and Ge Li. 2020. Deep image spatial transformation for person image generation. In *IEEE/CVF Conference on Computer Vision and Pattern Recognition*. 7690–7699.
- Olaf Ronneberger, Philipp Fischer, and Thomas Brox. 2015. U-net: Convolutional networks for biomedical image segmentation. In *International Conference on Medical Image Computing and Computer-Assisted Intervention*. 234–241.
- Sam T Roweis and Lawrence K Saul. 2000. Nonlinear dimensionality reduction by locally linear embedding. *Science* 290, 5500 (2000), 2323–2326.
- Patsorn Sangkloy, Jingwan Lu, Chen Fang, Fisher Yu, and James Hays. 2017. Scribbler: Controlling deep image synthesis with sketch and color. In *IEEE Conference on Computer Vision and Pattern Recognition*. 5400–5409.
- Kripasindhu Sarkar, Lingjie Liu, Vladislav Golyanik, and Christian Theobalt. 2021. HumanGAN: A Generative Model of Humans Images. *arXiv preprint arXiv:2103.06902* (2021).
- Kripasindhu Sarkar, Dushyant Mehta, Weipeng Xu, Vladislav Golyanik, and Christian Theobalt. 2020. Neural Re-Rendering of Humans from a Single Image. In *European Conference on Computer Vision*.
- Aliaksandr Siarohin, Enver Sangineto, Stéphane Lathuilière, and Nicu Sebe. 2018. Deformable gans for pose-based human image generation. In *IEEE Conference on Computer Vision and Pattern Recognition*. 3408–3416.
- Edgar Simo-Serra, Satoshi Iizuka, and Hiroshi Ishikawa. 2018. Mastering sketching: adversarial augmentation for structured prediction. *ACM Transactions on Graphics (TOG)* 37, 1 (2018), 1–13.
- Hao Tang, Song Bai, and Nicu Sebe. 2020a. Dual Attention GANs for Semantic Image Synthesis. In *ACM International Conference on Multimedia*. 1994–2002.
- Hao Tang, Dan Xu, Yan Yan, Philip HS Torr, and Nicu Sebe. 2020b. Local class-specific and global image-level generative adversarial networks for semantic-guided scene generation. In *IEEE/CVF Conference on Computer Vision and Pattern Recognition*. 7870–7879.
- Bochao Wang, Huabin Zheng, Xiaodan Liang, Yimin Chen, Liang Lin, and Meng Yang. 2018b. Toward characteristic-preserving image-based virtual try-on network. In *European Conference on Computer Vision*. 589–604.
- Ting-Chun Wang, Ming-Yu Liu, Jun-Yan Zhu, Andrew Tao, Jan Kautz, and Bryan Catanzaro. 2018a. High-resolution image synthesis and semantic manipulation with conditional gans. In *IEEE Conference on Computer Vision and Pattern Recognition*. 8798–8807.
- Jun-Yan Zhu, Taesung Park, Phillip Isola, and Alexei A Efros. 2017a. Unpaired Image-To-Image Translation Using Cycle-Consistent Adversarial Networks. In *IEEE Conference on Computer Vision and Pattern Recognition*. 2223–2232.
- Shizhan Zhu, Raquel Urtasun, Sanja Fidler, Dahua Lin, and Chen Change Loy. 2017b. Be Your Own Prada: Fashion Synthesis With Structural Coherence. In *IEEE International Conference on Computer Vision*.
- Zhen Zhu, Zhiliang Xu, Ansheng You, and Xiang Bai. 2020. Semantically Multi-modal Image Synthesis. In *IEEE/CVF Conference on Computer Vision and Pattern Recognition*. 5467–5476.